CARBON 50 (2012) 4640–4647

Available at www.sciencedirect.com

SciVerse ScienceDirect

journal homepage: www.elsevier.com/locate/carbon

The production of a cellular graphene array by scanning probe lithography and its ability to store electrical charge

Hyeondeuk Yong [a], *Kiyeol Kim* [a], *Wooseok Choi* [a], *Joonkyu Park* [a], *Muneer Ahmad* [b], *Yongho Seo* [a,b,*]

[a] *Faculty of Nanotechnology and Advanced Material Engineering and Graphene Research Institute, Sejong University, Seoul 143-747, South Korea*

[b] *Graphene Research Institute, Sejong University, Seoul 143-747, South Korea*

ARTICLE INFO

Article history:
Received 6 March 2012
Accepted 23 May 2012
Available online 31 May 2012

ABSTRACT

A graphene cellular array on an insulating SiO_2 layer was fabricated by scanning probe lithography. The graphene layer was oxidized by an electric field which was applied between the cantilever tip and Si substrate without any electrode directly connected to the graphene layer. When the bias voltage was applied on a cell of patterned graphene through the cantilever tip, charge was accumulated on the cell and preserved for a long time without decay. The accumulated charge and the surface potential were measured by an electrostatic force microscope. The charge retention was measured as a function of time, and the decay time constant was estimated to be ~70 min.

1. Introduction

Since graphene has emerged as a next generation device material [1,2], its patterning became a crucial issue for its industrial applications. Nanometer-scale high-resolution etching without chemical contamination is a main target of the graphene patterning, in order to control the band gap [3,4] and preserve its high mobility characteristic [5]. In general, e-beam lithography technique has some limitations to be used as a nano-patterning method: the spatial resolution of ~10 nm scale and chemical contamination from resist mask. On the other hand, scanning probe lithography (SPL) is considered as a promising candidate because the spatial resolution can be reduced as much as a few nm and no resist mask is required [6–8]. In this context, Tapaszto et al. fabricated 2.5 nm wide armchair graphene nano-ribbon by using scanning tunneling microscopy in air [7]. While many groups have performed the graphene patterning using SPL assisted by water under ambient conditions, Park et al., have succeeded in making 3 nm line width pattern in methanol environment [6]. They claimed that methanol provided a suitable environment for the graphene to be etched, because methanol has low viscosity and good wettability, and also it lowers the activation energy of the chemical reaction. In spite of these remarkable achievements on the graphene patterning, still there are limitations for SPL to be used as a general tool for patterning. One of the main problems is that the graphene layer should be connected to a counter electrode forming current path. In this study, we report the SPL patterning of graphene without direct connection to the electrode.

Recently, several papers have reported about the surface potential of graphene layer studied by electrostatic force microscopy (EFM) [9–18]. As EFM signal is very sensitive to the surface potential, it is used to study doping effect on the graphene which modifies the surface potential. Burnett et al. used EFM to identify the number of graphene layers where the topography was disturbed by adsorbates [11]. They developed EFM spectroscopy measuring the EFM phase as a

* *Corresponding author at:* Faculty of Nanotechnology and Advanced Material Engineering and Graphene Research Institute, Sejong University, Seoul 143-747, South Korea. Fax: +82 2 3408 4342.
E-mail address: yseo@sejong.ac.kr (Y. Seo).

0008-6223/$ - see front matter
http://dx.doi.org/10.1016/j.carbon.2012.05.051

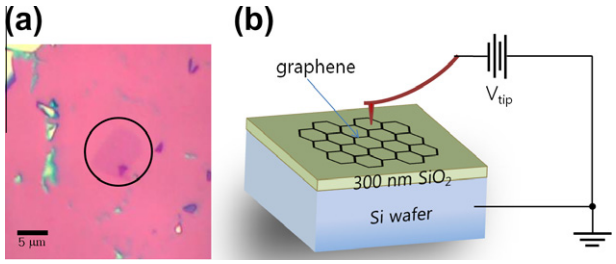

Fig. 1 – (a) Optical microscope image shows a single layer graphene deposited on a Si wafer with 300 nm SiO_2 layer. (b) Schematic diagram shows the setup for the SPL patterning. While the Si substrate was connected to the ground, graphene layer was not directly connected to the Si substrate.

function of the electrical DC bias to investigate the surface potential. Datta et al. reported EFM measurements revealing that a few-layer-graphene surface potential increases with film thickness, and it was saturated at five layers to the bulk graphite potential [10]. They attributed this effect to charge screening by graphene's relativistic low energy carriers. Very recently, graphite was patterned into hexagonal shape by Kurra et al., and charge storage effect was studied using EFM [12]. They found that the isolated topmost graphene island on the graphite substrate had charge storage behavior with unexpected stability of charged state. In this context, we patterned a graphene layer into a cellular array and each cell was studied by EFM spectroscopy and charging effect on each cell was investigated.

2. Experiments

Single layer graphene was prepared by mechanical exfoliation method from a highly oriented pyrolytic graphite using a 'Scotch tape'. The film was deposited on a Si wafer with 300 nm thick SiO_2 layer. Fig. 1a shows an optical microscope image of the sample on Si/SiO_2 substrate. In the patterning process, Si substrate was connected to the ground, and the

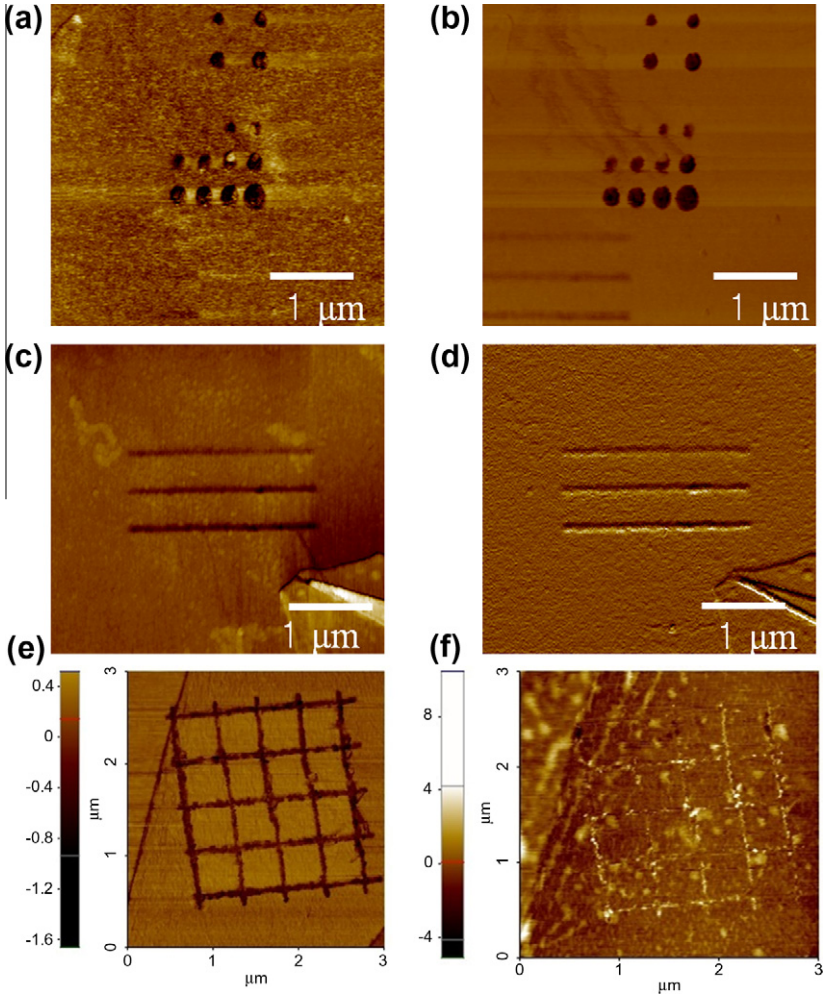

Fig. 2 – (a) Topography and (b) LFM images of dot patterns are shown. The tip bias voltages for writing were −12, −16, −20, and −24 V for upper four dots, and −8, −9.6, −11.2, −12,8, −14.4, −16.0, −19.2, −22.4, −25.6, −28.8, −32, and −40 V for lower 12 dots. (c) Topographic and (d) error images were measured after line patterning. Each line was drawn with different frequencies of square waveform: 100, 50, and 10 Hz, respectively. (e) LFM and (f) non-contact mode AFM images were taken for cellular array of graphene fabricated by combining the line drawings.

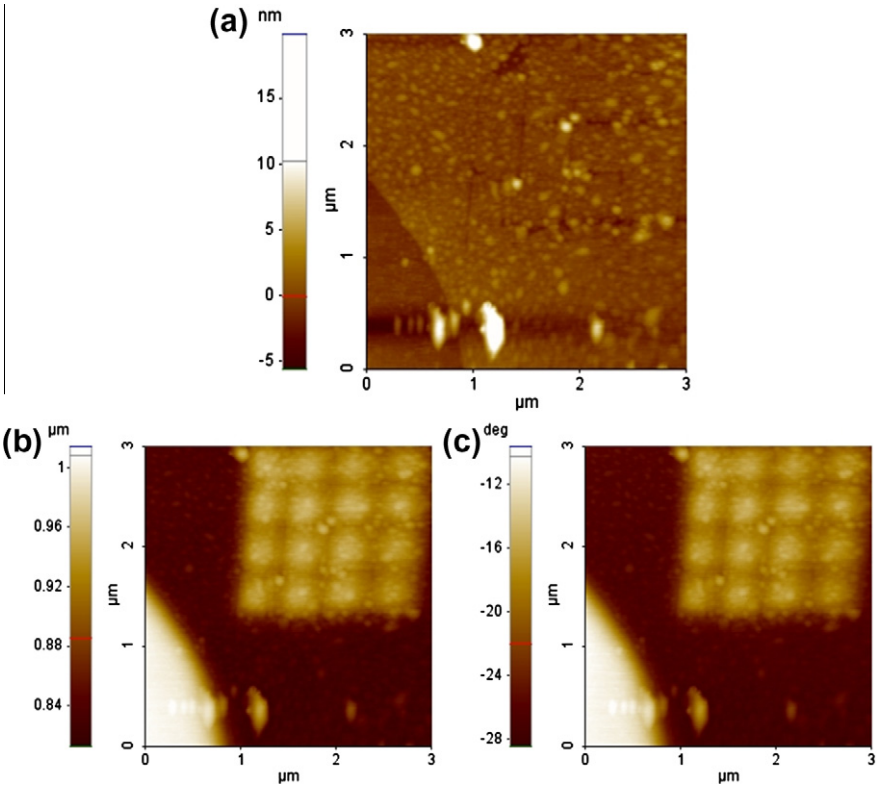

Fig. 3 – For a cellular graphene array, (a) non-contact mode topography and EFM images from (b) amplitude shift and (c) phase shift were measured simultaneously with tip-sample distance 16 nm and tip bias 2 V.

graphene layer was not connected to the Si substrate, as shown in Fig. 1b. A cantilever with conductive coating was biased with V_{tip}, which was contacted to the graphene layer. In this geometry, the resistance between the tip and Si substrate was larger than 10^9 Ω, and the current with ~10 V bias was less than 10 nA. For the scanning probe microscope, a commercial machine (XE-100, Park systems) was used under ambient conditions. In the patterning process, contact-mode scanning was employed, and for EFM measurement a two-pass method was used with ~10 nm lift height. To apply tip bias larger than 10 V, an external voltage source was connected manually to the cantilever. For the EFM, cantilever system (Multi 75E-G, Budget Sensors) with a 3 N/m force constant and 75 kHz resonant frequency was used, and the patterning was accomplished by Pt coated (CSG01/Pt, NT-MDT) cantilever.

For the writing process, negative voltages in square waveforms with 100 Hz frequency and time duration 5 s were applied to the tip. The peak-to-peak voltages V_{pp} were in the range from −8 to −40 V, and the writing speed was about 0.4 μm/s. This voltage scale is much higher than that when graphene layer was grounded directly. In this experiment the graphene was floated, so higher voltage was required to induce enough electric field to activate the chemical reaction. It should be noticed that a conductive coating on tip does not make electrical contact to the graphene surface due to surface oxidation on tip, unless it was pressed with a strong normal force.

3. Results and discussion

Some representative patterns written by the SPL are shown in Fig. 2. In Fig.2a contact mode topography and (b) lateral force microscopy (LFM), dot patterns were fabricated by bias voltage at fixed points. From the topography (a), the dots seem to be etched holes, but the contact mode image may have artifacts due to second order effect of frictional force, which was already discussed in the literature published by our group [8]. From the LFM image (b), the frictional force contrast is much clearer than the topography, but non-contact mode AFM image should be taken to measure the real topography. Line patterns were also fabricated by scanning with negative voltages, as shown in Fig. 2c topography and (d) error image. A cellular array of graphene was fabricated by combining the line drawings with the same conditions, as shown in Fig. 2e and f. From the LFM image (e), it is clear that each cell is separated by patterned lines, confirming the patterned parts exert large frictional force, again. However, the non-contact mode topography (f) shows that patterned surface is not smooth with some parts swelled partially. As the single-layer-graphene thickness is very thin (0.3 nm), the etched parts are not distinguishable, but the swelled parts are noticeable which is supposed to be oxidized with –O, or –OH group. It is well known that SPL on graphite causes etching or protrusion, depending on the voltage [8]. The carbons are oxidized by the activation energy provided from electric potential

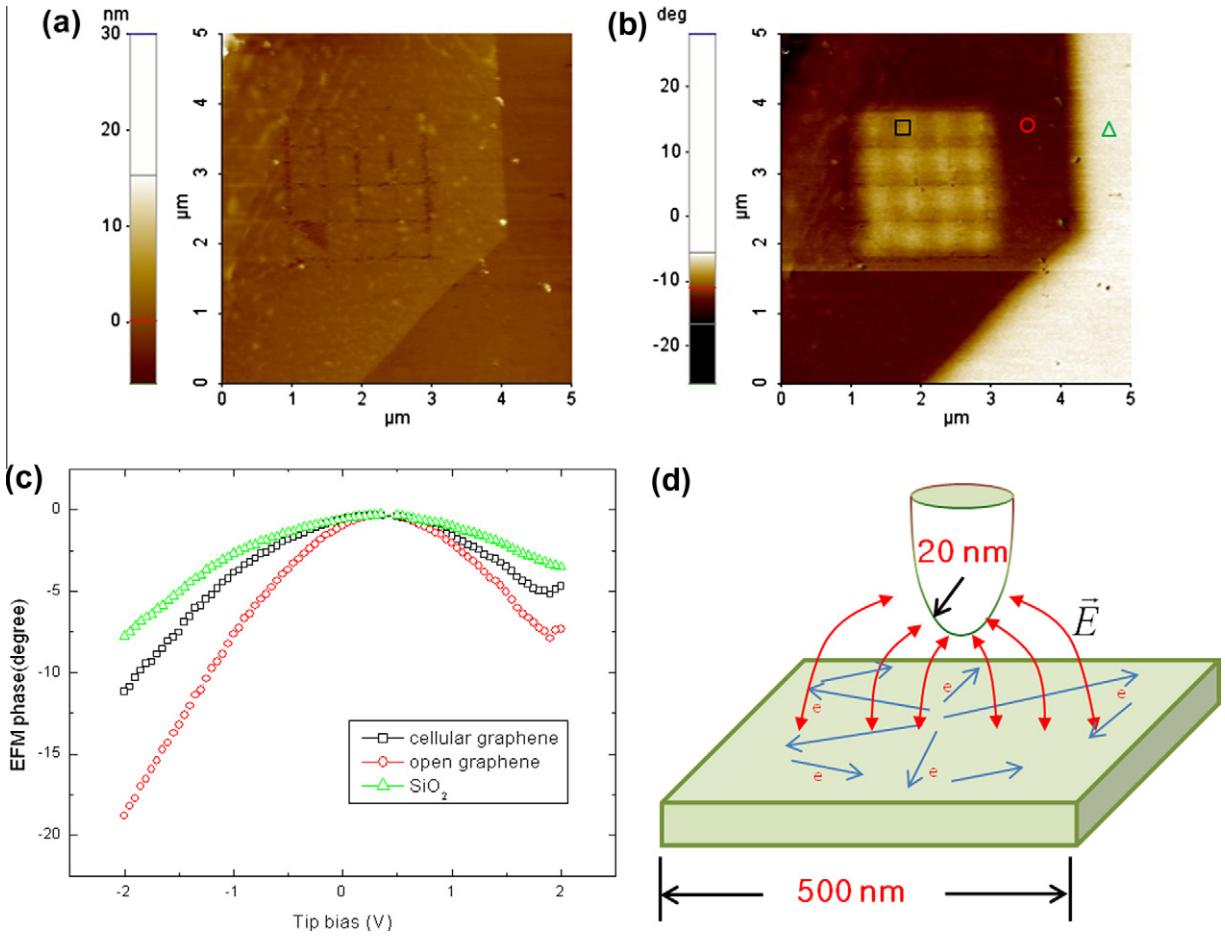

Fig. 4 – (a) Topography and (b) EFM images of the cellular graphene were taken simultaneously. (c) At three points indicated by symbols (□, ○, Δ), the EFM phase signal was collected as a function of the tip bias between −2 and +2 V. (d) This illustration shows that effective area of the capacitive coupling with a metallic probe is expanded by the ballistic motion of electrons in graphene.

energy. Depending on the voltage, the oxidized carbon either remains in the surface, or is gasified as CO, CO_2 [6,19]. In this experiment, the high voltages were applied, but all carbon atoms were not gasified judging from the topography.

In order to investigate the electric properties of the patterned cell of graphene, EFM measurements were carried out. Fig. 3 shows (a) non-contact mode topography, EFM images obtained from (b) amplitude and (c) phase, simultaneously measured with tip-sample distance 16 nm and tip bias 2 V. The amplitude image and phase image are almost identical, confirming that both images reflect the same physical properties eventually. The EFM contrast between the pristine graphene and patterned graphene (closed cell) is very clear. The SiO_2 layer at the left lower corner was not covered by the graphene, which has different brightness. The patterned lines with very high resistance disconnect the electrical conduction [12,20]. Judging from the EFM contrast, it is confirmed that each cell is isolated from the open graphene, having different capacitive coupling with the tip. As the SiO_2 layer is brightest and the graphene is darkest in EFM, it is presumed that the brightness is inversely proportional to its capacitive couplings.

We prepared another sample for the detailed analysis, and the EFM measurements were carried out more carefully. After the cellular patterning, (a) topography and (b) EFM images were taken simultaneously as shown in Fig. 4. At three selected points indicated by symbols (□, ○, Δ), the EFM phase signal was collected as the tip bias was swept between −2 V and +2 V. Each data set taken from the specific points was plotted in Fig. 4c. The EFM signal comes from the capacitive coupling force between the tip and sample mainly, which is given by Lei et al. [13].

$$F_{el} = \frac{1}{2}\frac{dC}{dz}(V_{tip} - V_s)^2 \quad (1)$$

where C is the capacitance between the tip and the sample, and V_s is the surface potential of the sample. Accordingly, phase signal of the EFM is given by

$$\Delta\phi \cong \frac{Q}{2k}\frac{d^2C}{dz^2}(V_{tip} - V_s)^2 \quad (2)$$

where Q is the quality factor and k is the spring constant of the cantilever.

The phase change data as a function of V_{tip} can be fitted to Eq. (2), and V_s can be estimated. From the phase spectrum in

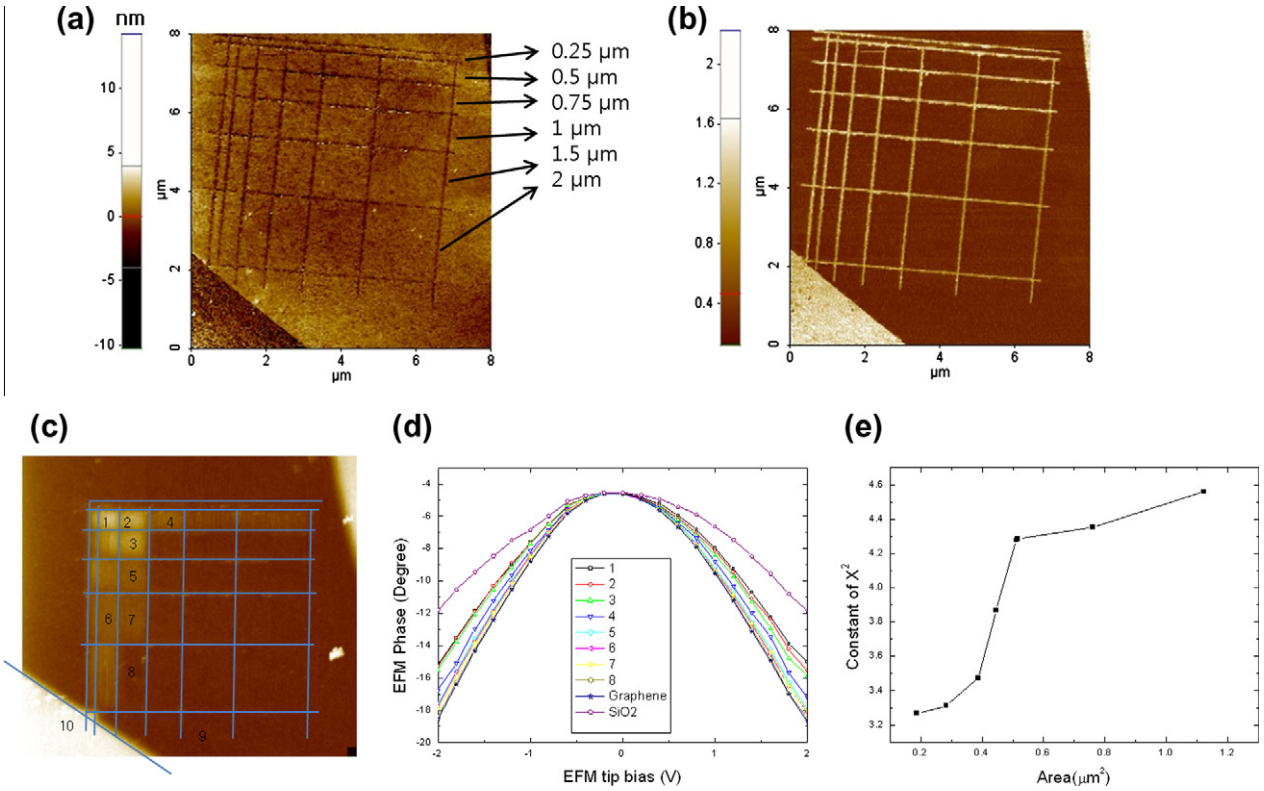

Fig. 5 – (a) Topography and (b) LFM images of cellular graphene fabricated with different sizes were taken simultaneously. (c) EFM image shows the different contrasts depending on the size of the cells. (d) EFM spectrum on each cell was measured, and (e) its curvature is plotted a function of cell area. The data show a saturation behavior for the cells larger than 0.5 μm².

Fig. 4c, local surface potential is estimated as 0.33, 0.42, and 0.36, (with standard deviation ±0.03) for cellular graphene, open graphene, and SiO_2, respectively. All positive values of V_s mean that the sample was *p*-type doped. This doping effect may likely be due to the residue of the sticky tape in the mechanical exfoliation process [15]. As the graphene is very sensitive to contamination, the V_s shift is larger than SiO_2 surface. However, in case of patterned part of graphene, the residue was supposed to be eliminated partially due to the chemical oxidation process, and the surface potential shift is reduced. The curvatures of the parabolic curves are quite different in the order: open > cellular > SiO_2. As the SiO_2 layer is insulating material, the smallest capacitance is plausible. In case of open graphene having largest effective area, the second derivative of capacitance in Eq. (2) was expected to be small, but the result was reversed. Therefore, we insist that the curvature is not only determined by the second derivative of the capacitance, but also it depends on the local conductivity, effective size or doping of the graphene. One possible explanation can be found in the fact that the cellular graphene has limited area for electrons to move without collision, while the electrons in open graphene may have ballistic motion with collision length ~500 nm [9,21,22]. Due to the ballistic motion of carriers in graphene, the capacitance between graphene and local probe has an effective area larger than the probe size (≈20 nm). The effective range affected by the capacitive coupling is expanded up to the mean free path of the graphene as illustrated in Fig. 4d. It is noted that the capacitance in this experiment means ac capacitance implying the electrons move dynamically synchronized with the cantilever motion. As a result, the hindered ballistic motion on cellular graphene decreases the capacitance with metallic probe.

Another cellular graphene array was fabricated with different cell sizes, as shown in Fig. 5a contact-mode topography and (b) LFM images. EFM results in Fig. 5c show different contrasts depending on the size of the cells. The small cell has bright contrast and large cell has dark contrast as a whole. Representative cells were numbered as indicated in Fig. 5c with the order of cell size, and EFM spectroscopy was measured for each cell as shown in Fig. 5d. The surface potential shift is not noticeable, but the parabolic curvatures are quite different. The curvatures are plotted as a function of the cell area as shown in Fig. 5e. While the curvature is increased as the cell size grows initially, for the cells with areas larger than 0.5 μm^2 it was saturated to the value of open graphene. This means that the cell size of ~700 nm is larger than the mean free path of electrons in graphene. This length scale is also in good agreement with the values reported by others [1,9,21,22].

Particular cells were charged by biased tip with writing voltage (V_w) in contact mode for 2 min and the EFM images were taken by the same biased tip with reading voltage (V_r), as shown in Fig. 6. Because the patterned boundary has large resistivity [23], the cell is expected to retain the charges. Fig. 6a and b shows EFM images taken after charging on the cells marked by circle with different V_w and V_r. These images show clear difference in charging status which confirms that the cells are charged and retained the charging status stably.

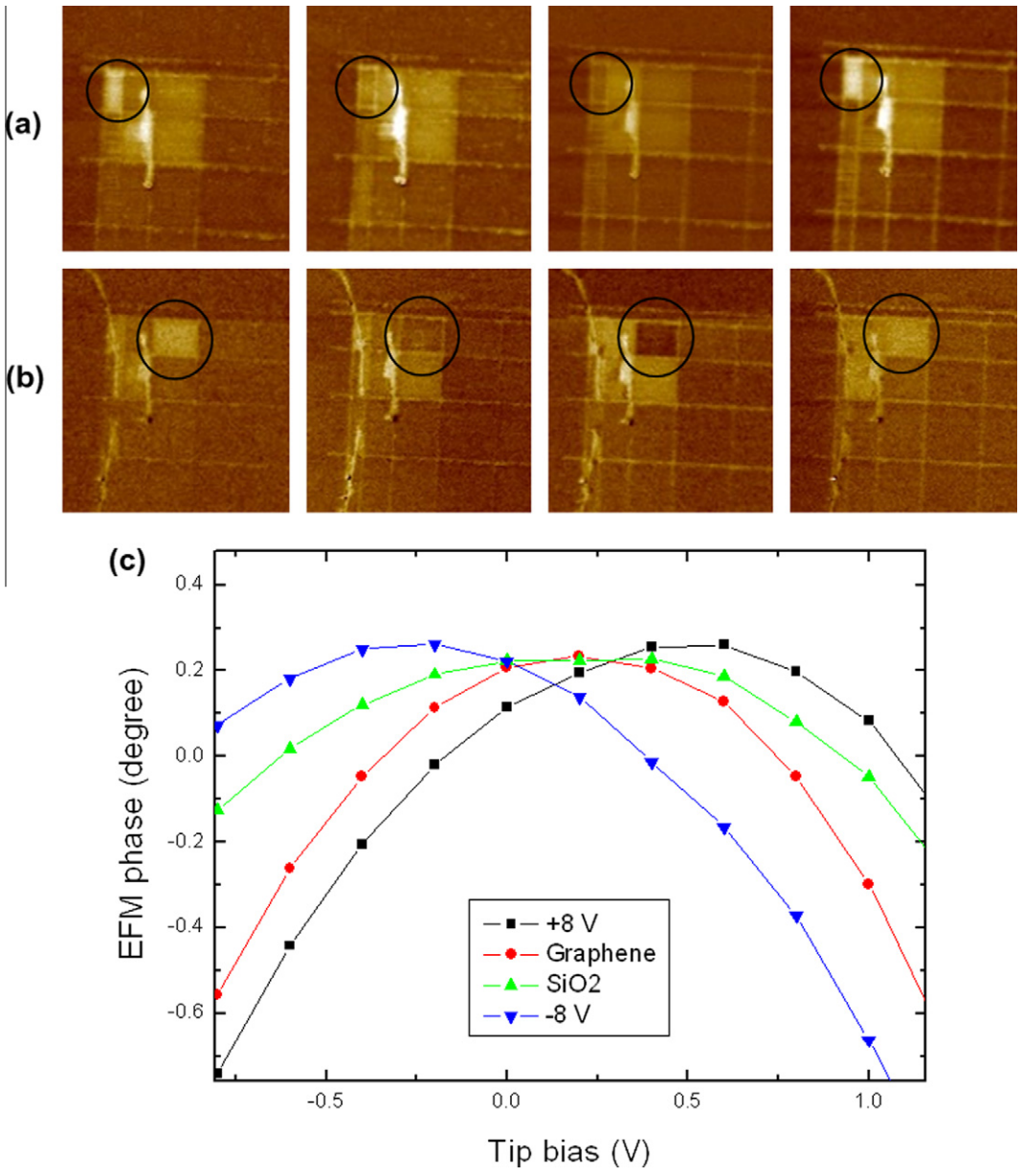

Fig. 6 – (a) and (b) show EFM images taken after charging on the cell marked by circle with different writing and reading voltages : (+8 V, +2 V), (−8 V, +2 V), (+8 V, −2 V), and (−8 V, −2 V), sequentially from left to right. (c) EFM spectra on the charged cell marked in (b) were measured. Some stains were made by unintended erroneous operations in the measurements.

On the charged cell, the EFM spectra were taken, as shown in Fig. 6c. As expected, the cell charged with positive bias (■) has positive surface potential +0.5 V and the negative biased cell (▼) has negative surface potential −0.25 V. The spectra for open graphene (●) and SiO_2 (▲) are shown here for comparison, which appear similar as already shown in Fig. 4c. The negatively (positively) charged cell possessed electron (hole) carrier which was injected from the biased tip. This charging effect occurred noticeably in the cells with areas from 0.06 μm^2 to 0.270 μm^2, but it was not distinguishable on the large area cells.

In order to study the time evolution on the charged cell, the EFM measurements were repeated for a long time period after the charging. The consecutive images show that the bright cell is gradually faded out with time, as shown in Fig. 7a. The time evolution was plotted as shown in Fig. 7b, where the contrast along y-axis was defined as a relative intensity compared to that of the SiO_2 (not shown). The data was fitted to an exponential decay function, and the best fitting results are shown by the red line. The reduced contrast means that the charge diffusion by leakage current, and the diffusion time constant was estimated as 70 min.

In general, when the charges injected in a localized area diffuse through conducting medium, they decay in an exponential form. From the continuity equation, the charge density as a function of time is given by

$$\rho_Q(t) = \rho_0 e^{-(\sigma/\varepsilon)t}, \quad (3)$$

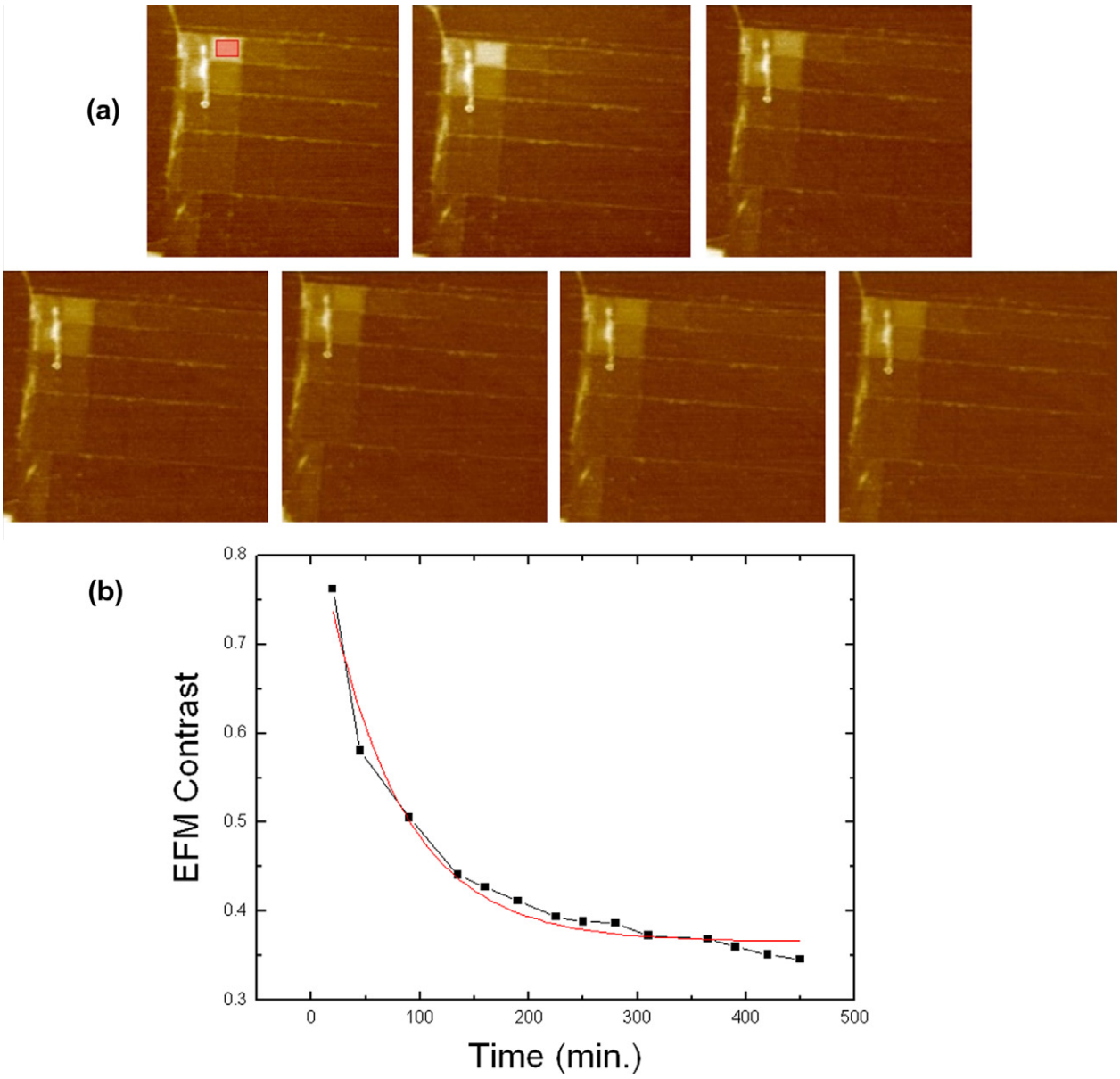

Fig. 7 – (a) Sequential images were taken at 5, 20, 90, 190, 280, 365, and 450 min, after charging on the cell marked (■). (b) The time evolution of the EFM contrast was plotted as a function of time, and was fitted to an exponential decay function marked with a red line. (For interpretation of the references to colour in this figure legend, the reader is referred to the web version of this article.)

where σ is the conductivity, ε is the dielectric constant, and the relaxation time τ is given by $\tau = \varepsilon/\sigma$. Assuming that the charge injected on the cell is a point charge and the oxidized graphene barrier is the surrounding uniform medium, the resistivity of the oxidized graphene is estimated as $\rho = \tau/\varepsilon \sim 10^{14}\,\Omega\,\mathrm{m}$, and the patterned part can be utilized as a good insulating barrier for the graphene-based electronic device.

4. Summary

We have prepared a cellular graphene device using SPL without directly connected electrode under ambient conditions. By using EFM, the capacitance of the individual cells was investigated as a function of the cell area. The ballistic motion of the electrons in the single layer graphene was confirmed, from the unexpected capacitance decrease of the cells with smaller area. The estimated mean free path of the electrons was about 500 nm. Charges were accumulated on isolated cellular graphene and the surface potential was measured by EFM. The time evolution of charge diffusion was measured, and the decay time constant was estimated to be 70 min. From the decay constant, the resistivity of the oxidized graphene was found as $\sim 10^{14}\,\Omega\,\mathrm{m}$. As a conclusion, SPL technique can be applied to fabricate the graphene-based electronic devices, and the charging effect on the cellular graphene can be utilized in memory devices.

Acknowledgments

This research was supported by Basic Science Research Program (2009-0070725, 2010-0005393) and Priority Research Centers Program (2012–0005859) through NRF funded by MEST.

Appendix A. Supplementary data

Supplementary data associated with this article can be found, in the online version, at http://dx.doi.org/10.1016/j.carbon.2012.05.051.

REFERENCES

[1] Geim AK, Novoselov KS. The rise of graphene. Nat Mater 2007;6(3):183–91.
[2] Avouris P, Chen ZH, Perebeinos V. Carbon-based electronics. Nat Nanotechnol 2007;2(10):605–15.
[3] Son Y-W, Cohen ML, Louie SG. Energy gaps in graphene nanoribbons. Phys Rev Lett 2006;97:216803.
[4] Chen Z, Lin Y-M, Rooks MJ, Avouris P. Graphene nano-ribbon electronics. Physica E 2007;40:228–32.
[5] Novoselov KS, Geim AK, Morozov SV, Jiang D, Katsnelson MI, Grigorieva IV, et al. Two-dimensional gas of massless Dirac fermions in graphene. Nature 2005;438(7065):197–200.
[6] Park J, Kim KB, Park JY, Choi T, Seo Y. Graphite patterning in a controlled gas environment. Nanotechnology 2011;22(33):335304.
[7] Tapaszto L, Dobrik G, Lambin P, Biro LP. Tailoring the atomic structure of graphene nanoribbons by scanning tunnelling microscope lithography. Nat Nanotechnol 2008;3(7):397–401.
[8] Yong H, Lee H, Kim KB, Lee NS, Seo Y. Application of scanning probe lithography to graphite patterning. J Nanosci Nanotechnol 2011;11(2):1397–400.
[9] Berger C, Song Z, Li X, Wu X, Brown N, Naud C, et al. Electronic confinement and coherence in patterned epitaxial graphene. Science 2006;312(5777):1191–6.
[10] Datta SS, Strachan DR, Mele EJ, Johnson AT. Surface potentials and layer charge distributions in few-layer graphene films. Nano Lett 2009;9(1):7–11.
[11] Burnett T, Yakimova R, Kazakova O. Mapping of local electrical properties in epitaxial graphene using electrostatic force microscopy. Nano Lett 2011;11(6):2324–8.
[12] Kurra N, Prakash G, Basavaraja S, Fisher TS, Kulkarni GU, Reifenberger RG. Charge storage in mesoscopic graphitic islands fabricated using AFM bias lithography. Nanotechnology 2011;22(24):245302.
[13] Lei CH, Das A, Elliott M, Macdonald JE. Quantitative electrostatic force microscopy-phase measurements. Nanotechnology 2004;15(5):627–34.
[14] Lu Y, Munoz M, Steplecaru CS, Hao C, Bai M, Garcia N, et al. Electrostatic force microscopy on oriented graphite surfaces: coexistence of insulating and conducting behaviors. Phys Rev Lett 2006;97(7):076805.
[15] Moser J, Verdaguer A, Jimenez D, Barreiro A, Bachtold A. The environment of graphene probed by electrostatic force microscopy. Appl Phys Lett 2008;92(12):123507.
[16] Shi YM, Dong XC, Chen P, Wang JL, Li LJ. Effective doping of single-layer graphene from underlying SiO(2) substrates. Phys Rev B 2009;79(11):115402.
[17] Singh MK, Titus E, Goncalves G, Marques PA, Bdikin I, Kholkin AL, et al. Atomic-scale observation of rotational misorientation in suspended few-layer graphene sheets. Nanoscale 2010;2(5):700–8.
[18] Zhao MH, Gu XH, Lowther SE, Park C, Jean YC, Nguyen T. Subsurface characterization of carbon nanotubes in polymer composites via quantitative electric force microscopy (vol. 21, 225702, 2010). Nanotechnology 2010;21(33):225702.
[19] Hiura HF. Tailoring graphite layers by scanning tunneling microscopy. Appl Surf Sci 2004;222(1–4):374–81.
[20] Byun IS, Yoon D, Choi JS, Hwang I, Lee DH, Lee MJ, et al. Nanoscale lithography on monolayer graphene using hydrogenation and oxidation. ACS Nano 2011;5(8):6417–24.
[21] Areshkin DA, Gunlycke D, White CT. Ballistic transport in graphene nanostrips in the presence of disorder: importance of edge effects. Nano Lett 2007;7(1):204–10.
[22] Novoselov KS, Geim AK, Morozov SV, Jiang D, Zhang Y, Dubonos SV, et al. Electric field effect in atomically thin carbon films. Science 2004;306(5696):666–9.
[23] Weng L, Zhang L, Chen YP, Rokhinson LP. Atomic force microscope local oxidation nanolithography of graphene. Appl Phys Lett 2008;93:093107.